2003

Reversing Circulation Patterns in a Tropical Estuary

Arnoldo Valle-Levinson
Old Dominion University

Kathryn T. Bosley

Original Publication Citation

Valle-Levinson, A., & Bosley, K. T. (2003). Reversing circulation patterns in a tropical estuary. *Journal of Geophysical Research: Oceans, 108*, 3331. doi:10.1029/2003jc001786

Reversing circulation patterns in a tropical estuary

Arnoldo Valle-Levinson

Center for Coastal Physical Oceanography, Department of Ocean, Earth and Atmospheric Sciences, Old Dominion University, Norfolk, Virginia, USA

Kathryn T. Bosley

National Ocean Service, National Oceanographic and Atmospheric Administration, Chesapeake, Virginia, USA

Received 16 January 2003; revised 30 May 2003; accepted 18 June 2003; published 21 October 2003.

[1] A combination of current velocity and water density measurements was used to characterize the basic patterns of water exchange in the Gulf of Fonseca, a tropical estuary on the Pacific Ocean side of Central America. The measurements were obtained during spring and neap tides in March (dry season) and June (wet season) of 2001 and consisted of profiles of current velocity and density along four transects. From mid-March to mid-April a time series of hourly surface current velocity maps was also obtained with a high-frequency radar system of two antennas. The sampling transects and the radar coverage concentrated in the portion of the estuary that has open communication with the ocean. During the dry season, water exchange at the entrance to the gulf suggested an inverse estuarine circulation that was more robust, and its dynamics were closer to geostrophy during neap than during spring tides. It is likely that salinity increased toward the tributaries of the system and then decreased within those tributaries because of the persistent influence of fresh water. In contrast, during the wet season, salinity decreased into the estuary, and the circulation resembled that of a typical estuary. In this season the fortnightly modulation of exchange flows was masked by wind effects, which also played a relevant role in the dynamics. The net volume inflows measured in both seasons suggested that the residence time of the Gulf of Fonseca varies from 2 weeks to 1 month. *INDEX TERMS:* 4235 Oceanography: General: Estuarine processes; 4227 Oceanography: General: Diurnal, seasonal, and annual cycles; 4203 Oceanography: General: Analytical modeling; *KEYWORDS:* reversing estuarine circulation, Gulf of Fonseca, tropical estuary, Coriolis effects

Citation: Valle-Levinson, A., and K. T. Bosley, Reversing circulation patterns in a tropical estuary, *J. Geophys. Res.*, *108*(C10), 3331, doi:10.1029/2003JC001786, 2003.

1. Introduction

[2] Near Halloween (31 October) of 1998, Hurricane Mitch hit Central America. The hurricane moved very slowly through Honduras, Nicaragua, and El Salvador, producing widespread devastation from the excessive rains that accompanied the cyclone. In the aftermath, one priority identified by different government and private sector authorities from the countries affected was to understand the circulation in the Gulf of Fonseca, on the Pacific Ocean coastline of those countries (Figure 1). An improved understanding of the circulation is needed to aid fisheries and aquaculture management. Being a tropical estuary, the Gulf of Fonseca is subject to seasonal atmospheric forcing from contrasting wind and precipitation regimes and to fortnightly tidal forcing. Given these characteristic temporal scales of forcing, the general objective of this investigation was to characterize the circulation in a tropical estuary (1) from spring to neap tides and (2) from dry to wet seasons. The specific questions to address were, Do exchange patterns at the entrance to this tropical estuary persist (1) from spring to neap tides and (2) from the dry season to the wet season? These inquiries were tackled with observations of current velocity and density profiles and with surface maps of currents. These technical approaches have rarely been used in tropical systems. Several studies in subtropical or semiarid systems have already documented fortnightly tidal modulation of net water exchange [e.g., *Nunes and Lennon*, 1987; *Nunes Vaz et al.*, 1989, 1990]; this has also been studied in temperate systems [e.g., *Haas*, 1977; *Geyer and Cannon*, 1982; *Griffin and LeBlond*, 1990]. However, this effort constitutes one of the few in tropical estuaries that explores fortnightly and seasonal variability of water exchange patterns and one of the few examples that illustrates reversing water exchange patterns from season to season [e.g., *Valle-Levinson et al.*, 2001].

2. Area of Study

[3] The Gulf of Fonseca is located at 13°N on the Pacific side of Central America (Figure 1). It is a relatively large embayment, with a surface area of ~1600 km^2. The width at the entrance is ~40 km and spans from El Salvador to

0148-0227/03/2003JC001786

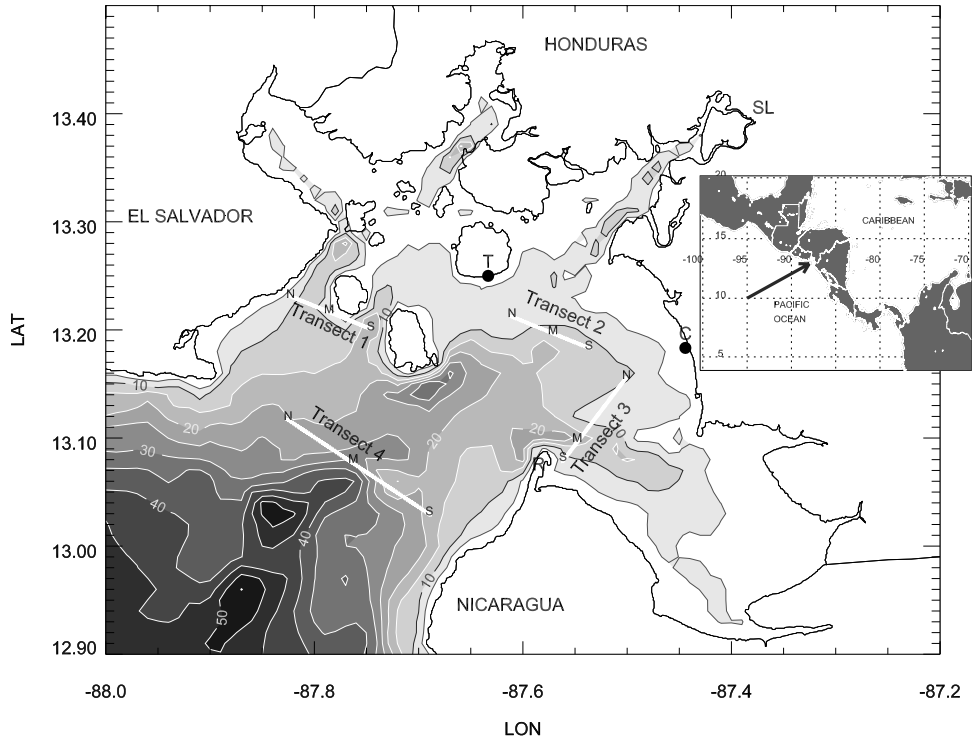

Figure 1. Map of the Gulf of Fonseca in Central America and location of sampling transects and radar sites. The radar sites are shown as black dots: T, El Tigre; and C, Cedeño. Bathymetry is contoured at 5 m intervals. R, Punta Rosario; SL, San Lorenzo; N, conductivity-temperature-depth recorder (CTD) station at the north of the transect; M, CTD station at the middle of the transect; S, CTD station at the south of the transect.

Nicaragua. The length from the entrance of the gulf to the head at San Lorenzo is ~60 km. The rivers still extend farther inland, but the upstream extent of saltwater intrusion and tidal oscillations is essentially unknown. The waters of the gulf are shared by three countries, El Salvador, Honduras, and Nicaragua, but the waters at the mouth are divided only between El Salvador and Nicaragua. The radial branching into four tributaries, the sharp bathymetry changes, and the scattered islands complicate the morphology of the gulf and are expected to shape a complex circulation.

[4] The volume of river discharge into the gulf is also unknown but is anecdotally present throughout the year. The most important rivers are the Choluteca in Honduras and the Goascorán, which separates Honduras and El Salvador. River discharge features a strong seasonality that reflects annual precipitations of ~2400 mm. Most rainfall occurs during the wet season that extends from May to October and is characterized by northeasterly to easterly moist winds related to the Caribbean Trades. The dry season spans from November to April and is dominated by southwesterly winds with episodic energetic northerly winds.

[5] The tides are predominantly semidiurnal, with an average tidal range of 2.5 m. The dominant tidal constituents are M_2, N_2, and S_2, which yield a marked fortnightly modulation with monthly asymmetry. This means that the difference between spring and neap tidal ranges within a single month is quite different in consecutive spring and neap tides.

[6] The mean depth of the gulf is ~15 m and the volume of the basin is $\sim 2.4 \times 10^{10}$ m^3. This represents, for example, ~60% of the volume of the Chesapeake Bay (3.9×10^{10} m^3 [*Salas-Monreal*, 2002]). Given the seasonal variability in buoyancy forcing and the fortnightly variability in tidal forcing, we sought to characterize the circulation patterns in the Gulf of Fonseca, a tropical estuary, considering these two temporal scales.

3. Data Collection and Analysis

[7] During the dry season, profiles of water velocity, temperature, salinity, and density were combined with maps of sea surface currents to characterize the basic patterns of subtidal exchange between the estuary and the adjacent Pacific Ocean waters. In the wet season these patterns were determined only with profiling data. Profiling data were obtained with a towed, RD Instruments 614.4 kHz acoustic Doppler current profiler (ADCP) and a SeaBird SBE-19 conductivity-temperature-depth recorder (CTD). Surface maps of currents were derived with two High-Frequency (HF) Coastal Radar (CODAR) antennas: SeaSondes.

[8] Profiling data were collected from the Nicaraguan vessel *Nolan Ponce* of the Empresa Portuaria Nacional during March (dry season) and June (wet season) of 2001. Velocity profiles were recorded along four transects (1, 2, 3, and 4 (Figure 1)) during spring and neap tides of the dry and wet seasons. Transect locations were designed to capture the flow patterns at the embayments that branch off from the main entrance to the estuary. Their position was ultimately determined by bathymetric constraints represented by the 1.8-m draft of the *Nolan Ponce*. Each of the

Table 1. Sampling Scheme[a]

Transect	ADCP and CTD Sampling, hours	Spring Tides[b] (Start Time, UTC)	Neap Tides[b] (Start Time, UTC)	ADCP 1st Bin, m	Bin Size, m	Average Interval, s
		Dry Season (March 2001)				
1	13	11 (2000)	18 (1300)	1.6	0.5	30
2	13	14 (1600)	20 (1400)	1.6	0.5	30
3	13	12 (1700)	19 (1600)	1.6	0.5	30
4	25	9–10 (1700)	16–17 (1400)	2.0	1.0	45
		Wet Season (June 2001)				
1	13	25 (1300)	15 (2100)	1.4	0.5	45
2	13	24 (1300)	17 (0000)	1.4	0.5	45
3	13	23 (1400)	18 (1600)	1.4	0.5	45
4	25	21–22 (1500)	14–15 (1500)	2.0	1.0	45

[a]ADCP, acoustic Doppler current profiler; CTD, conductivity-temperature-depth.
[b]Day (and start time) of each experiment. Local time is UTC - 6 hours.

four transects was sampled separately throughout a diurnal cycle (transect 4) or a semidiurnal tidal cycle (see Table 1). The length of the transect was determined in such a way that it could be repeated at least 8 times throughout the sampling period so that tidal and nontidal signals could be separated satisfactorily. The whole data set reflects a total of 16 separate experiments (Table 1).

[9] Water velocity profiles were obtained with the ADCP mounted on a 1.2-m-long catamaran that was towed from the starboard side at speeds of $\sim$2.5 m s^{-1}. The ADCP recorded velocity profiles at a rate of $\sim$10 pings averaged over 30 or 45 s according to the transect sampled (Table 1), which yielded a spatial resolution of 75–90 m. The bin size for vertical resolution was 0.5 or 1 m, again, depending on the transect. These settings were established by the different depth distributions of the transects. Navigation data were obtained with a Garmin GPSMAP 185 GPS and were used to calibrate the ADCP compass following *Joyce* [1989]. Data from the ADCP were also trimmed with the criteria outlined by *Valle-Levinson and Atkinson* [1999]. Corrected ADCP measurements were interpolated onto a uniform grid of 100 m in the horizontal and 0.5 m in the vertical, using Delaunay triangulations [*Fang and Piegl*, 1992, 1993]. Subtidal flows V_0 were determined at each grid point from a least squares fit of semidiurnal and diurnal (at transect 1 only) harmonics plus a subtidal contribution V_0 to the observations V, i.e., through minimization of the difference between both sides of the following relationship:

$$V = V_0 + V_2 \sin(\omega_2 t + \varphi_2) + V_1 \sin(\omega_1 t + \varphi_1),$$

where V is the vector of observations with east and north components (u, v). Furthermore, $V_{2,1}$ are the amplitudes of the semidiurnal and diurnal tidal currents, $\omega_{2,1}$ are the semidiurnal (2π/12 h) and diurnal (2π/24 h) frequencies, and $\varphi_{1,2}$ are the phases of both constituents relative to midnight (UT) of the day of the first experiment of the season (dry or wet). The main interest here is in the description of the subtidal contribution V_0.

[10] Water temperature, salinity, and density profiles were obtained at stations located at both ends and in the middle, or at the deepest part, of each ADCP transect (Figure 1). These stations were occupied during every transect repetition. The data were processed following the protocol of the instrument's manufacturer to align the sensors and eliminate loops while the CTD was lowered to the bottom. The mean profiles of temperature, salinity, and density are reported here for each of the three sampling points of every transect. These mean profiles are used to characterize the spatial distribution of properties in the lower part of the estuary and to infer the flow patterns expected from such distribution. Profiles of hydrographic properties are unavailable in the neap tides experiment of the dry season because of damage to the CTD.

[11] Surface currents were recorded every hour during the period between 10 March 2001 at 1500 UT and 14 April 2001 at 1300 UT. These currents were derived from radial measurements obtained by two land-based HF CODAR antennas of 25 MHz separated by 21 km. One antenna was located approximately in the middle of the estuary, on the southern shore of Tigre Island, Honduras (Figure 1), at 13°15′N, 87°38′W. The second antenna was deployed in the town of Cedeño, Honduras, at 13°11′N, 87°27′W (Figure 1). The grid size of the maps generated by the antennas was $\sim$1 km^2. There were several data gaps of between 1 hour and 2 days owing to power outages. Out of 839 hourly frames that would have been generated from the uninterrupted operation of the radars in almost 35 days, a total of 571 frames of good quality were recorded, i.e., a 68% return. Also, the spatial coverage expected from the antennas' range was slightly reduced by the presence of islands and capes (e.g., Punta Rosario in Nicaragua). Only one of the ADCP transect trajectories (transect 3) overlapped with the coverage provided by the antennas. However, the days of ADCP sampling of transect 3 were plagued with CODAR data gaps that hampered a strict comparison between the two current measuring techniques. Daily averages of CODAR data collected the day after ADCP transect 3 coverage showed overall qualitative agreement between the two methods. For the purpose of this study the 571 frames recovered from the radars' deployment were averaged to produce the mean surface flow field representative of the month of deployment. The CODAR antennas were not available for deployment in this area during the wet season.

4. Data Description

[12] During the dry season, hydrographic data (salinity, temperature, and density mean profiles) and month-long surface currents, but mainly ADCP measurements, suggested a pattern of inverse estuarine circulation in the Gulf of Fonseca. The inverse estuarine circulation pattern was

slightly modified from spring to neap tides but was better defined at neap tides. During the wet season, hydrographic data and mainly ADCP data suggested a pattern typical of estuarine conditions. This pattern was also mildly altered from neap to spring tides. The measurements obtained during dry and wet seasons are now expanded in a structure that follows the sequence just outlined.

4.1. Dry Season

[13] The average profiles of salinity, temperature, and density obtained at each station and transect sampled during spring tides are shown in Figure 2. The transect at the mouth of the gulf (transect 4) showed a general increase of salinity and water density from Nicaragua to El Salvador, i.e., from southeast to northwest (near-bottom increase of 0.5 kg m^{-3} in 20 km). In turn, the profiles at transect 3 showed larger values toward the north of the transect at the Honduras end than at the southern end in Nicaragua (see Figure 1). The hydrographic distributions at transects 2 and 1 showed a general water density increase, although weak, toward the north and west within each transect. Transect to transect comparisons displayed a slight increase in water density from transect 3 to transect 1. Comparisons to transect 4 can be misleading because this transect reflected mean temperatures and densities of a 25-hour period of sampling (Table 1), which included night cooling. Transects 1–3 reflected 13-hour periods (Table 1) sampled mostly during daytime hours, which biased the mean temperature and density profiles and jeopardized any comparison to transect 4. Salinity seemed to increase, in general, from transects 3 to 1, i.e., from east to west inside the lower gulf. This salinity increase inside the lower gulf must favor several salt farms observed throughout the coastal regions in Honduras and should also probably reflect an along-estuary increase in salinity and density, which was not really observable with our sampling strategy. As mentioned in section 3, hydrographic profiles were unavailable during neap tides.

[14] The main message of the hydrography average profiles during the dry season was that the transverse density gradient exhibited vertical and lateral variability. Near the bottom, density increased from east to west in the lower gulf with a representative transverse density gradient ($\partial\rho/\partial y$) of 2.5×10^{-5} kg m^{-4}. The along-estuary density gradient ($\partial\rho/\partial x$) was not really resolved by our measurements, but the gradients within transect 3 suggested that this gradient may have been similar (0.15–0.20 kg m^{-3} in 10 km in Figure 2) to the near-bottom transverse gradient. It is likely that at some point farther toward the head of the gulf the horizontal gradients of salinity and density would reverse sign in the regions of influence of the Goascarán River in El Salvador and the Choluteca River in Honduras. The slightly fresher surface layer in transect 2 (Figure 2) might reflect such freshwater influence and sign reversal. Still, in the lower part of the estuary, where our measurements concentrated, we should probably expect inverse estuarine conditions. In the estuary as a whole we should not rule out the possibility of this system behaving as a salt plug estuary [*Wolanski*, 1986]. The suggested inverse estuarine behavior in the lower estuary is further explored with the current velocity measurements.

[15] The average surface currents derived from the two HF radar sites are shown in Figure 3 for the almost 35 days of deployment from mid-March to mid-April 2001. The mean currents showed the strongest values off Punta Rosario and were directed into the gulf. The mean flow to the west and northwest of Punta Rosario indicated positive relative vorticity ($\partial v/\partial x - \partial u/\partial y$) and to the east and northeast showed negative relative vorticity (Figure 3b). In addition, the horizontal divergence of the mean currents ($\partial u/\partial x + \partial v/\partial y$) featured positive values right off Punta Rosario and convergences at either side. Such distributions of relative vorticity and horizontal divergence around a headland have been shown in other observations [*Geyer and Signell*, 1990; *Signell and Harris*, 2000] and have been attributed to tidal rectification in the vicinity of this morphological feature. The central message, however, of the mean flow distribution resolved by the radars was that the surface waters of the gulf moved into the system. These mean flows suggested a pattern of inverse estuarine circulation or, at least, surface inflow. The suggestions of inverse estuarine conditions are confirmed with the mean flow distributions measured with the towed ADCP.

[16] During spring tides the transect at the entrance to the Gulf of Fonseca (transect 4) featured net surface inflow and net bottom outflow (Figure 4a). Overall, the other three transects sampled in subsequent days exhibited a pattern that was, in general, consistent with that of a typical inverse estuary (e.g., Spencer Gulf in Australia [*Nunes Vaz et al.*, 1990]). There were some recirculations identified in transects 3, 2, and 1 that modified the inverse estuarine circulation pattern. These modifications reflected bathymetric effects, island wakes, and eddies around a cape, i.e., nonlinear influences in most cases. During neap tides the inverse estuarine pattern was preserved in every transect (Figure 4b), and mean recirculations were weaker than during spring tides but were still evident. This was a consequence of the reduction of tidally induced nonlinearities in neap tides. Of particular relevance to the water exchange pattern is the distribution of the mean flows at the entrance to the gulf (transect 4).

[17] The cross section of net along-estuary (u) flows at transect 4 featured well-defined Earth rotation effects, as the isotachs (isolines of velocity) tilted in the sense expected from Coriolis accelerations, i.e., upward from left to right looking seaward (Figure 5). The tilt of the isotachs was greater during spring tides (Figure 5a) than during neap tides (Figure 5b). This was likely a consequence of increased frictional and advective effects during spring tides because wind speeds were very low and essentially the same during spring and neap tides (Table 2). In fact, the tilt of the zero isotach (interface between net inflows and outflows) was closer to the geostrophic prediction derived from Margules's relation during neap tides than during spring tides. Margules's relation says that [*Gill*, 1982]

$$\alpha = \frac{f\rho_2(u_2 - u_1)}{g(\rho_2 - \rho_1)},$$

where α is the slope of the interface; u_1 and u_2 are the inflowing upper layer typical speed (0.15 m s^{-1}) and the outflowing lower layer typical speed (−0.05 m s^{-1}), respectively; ρ_1 and ρ_2 are the typical water densities of the upper (1022 kg m^{-3}) and lower (1023 kg m^{-3}) layers, respectively; and f is the Coriolis parameter for a latitude of

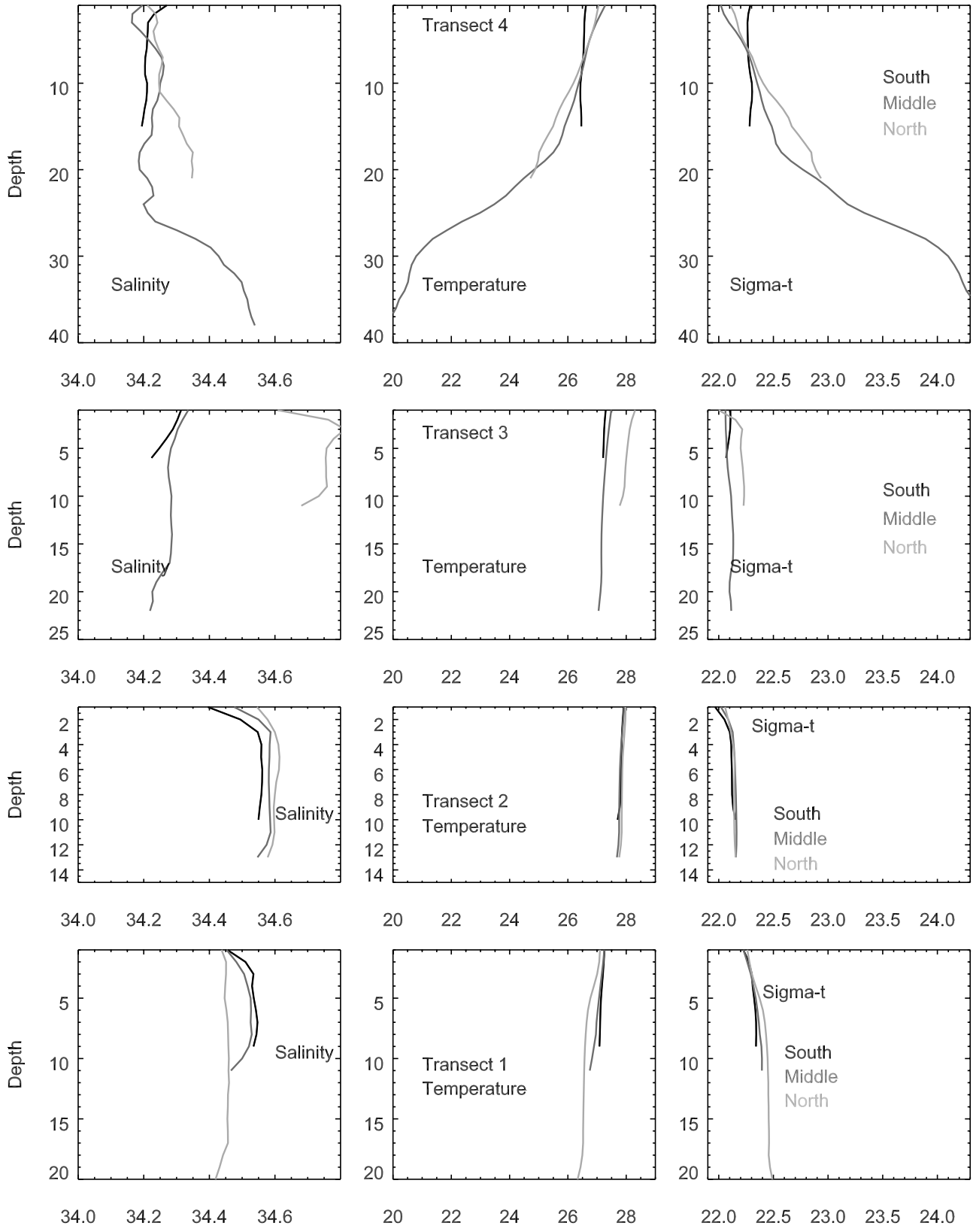

Figure 2. Mean salinity, temperature, and density anomaly profiles at the three sampling stations of each transect. Refer to Figure 1 for the location of the north, middle, and south station locations at each transect.

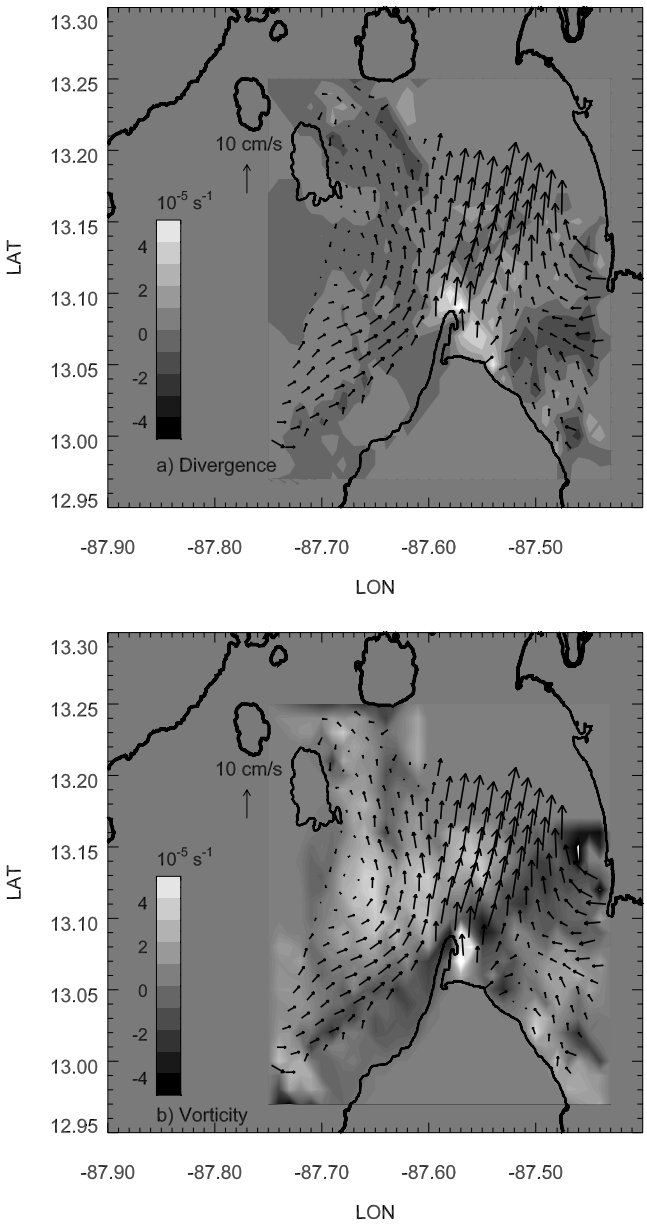

Figure 3. Mean surface velocity fields derived from the HF radar deployment during the month-long deployment, represented by the vectors used to plot contours of (a) divergence and (b) relative vorticity.

13°N (3.3×10^{-5} s^{-1}). The theoretical value of α was 7×10^{-4} or 7 m in 10 km, whereas the observed slope of the zero isotach in spring tides was 14×10^{-4} or 14 m in 10 km. In contrast, the slope of the zero isotach in neap tides was 10×10^{-4} or 10 m in 10 km. This highlights the slight modification by frictional effects during spring tides and the essentially geostrophic transverse dynamics of the exchange flow during neap tides.

[18] In addition to the diagnostic Margules's relation, the subtidal exchange hydrodynamics can be characterized through steady, linear dynamics as presented by *Kasai et al.* [2000] and *Valle-Levinson et al.* [2003] (see Appendix A for an explanation of an analytical model of these characteristics). Essentially, the subtidal hydrodynamics are assumed to be represented by a balance between the pressure gradient (with both barotropic and baroclinic contributions), frictional effects, and Coriolis accelerations. In this approach, under any bathymetric distribution across the estuary the competition between friction and Coriolis, characterized by the vertical Ekman number E, determines the shape of the exchange flows. Under low E, Coriolis dominates over friction, and the exchange is fundamentally geostrophic as portrayed by a two-layer circulation modified by the Earth's rotation. In contrast, under high E, friction dominates over Coriolis, and exchange flows are symmetric about a vertical axis in the middle of the channel [e.g., *Wong*, 1994]. The shape of the subtidal exchange at the entrance to the Gulf of Fonseca is best portrayed by the analytical solution with low E (Figure 5c) for neap tides. These results emphasize the negligible effects of friction in neap tides at the site and the slightly increased influence in spring tides.

[19] The scaling of dynamic terms (Table 2) and analytical model results (Figure 5c) indicated that the dynamics of both flow components were nearly geostrophic during neap

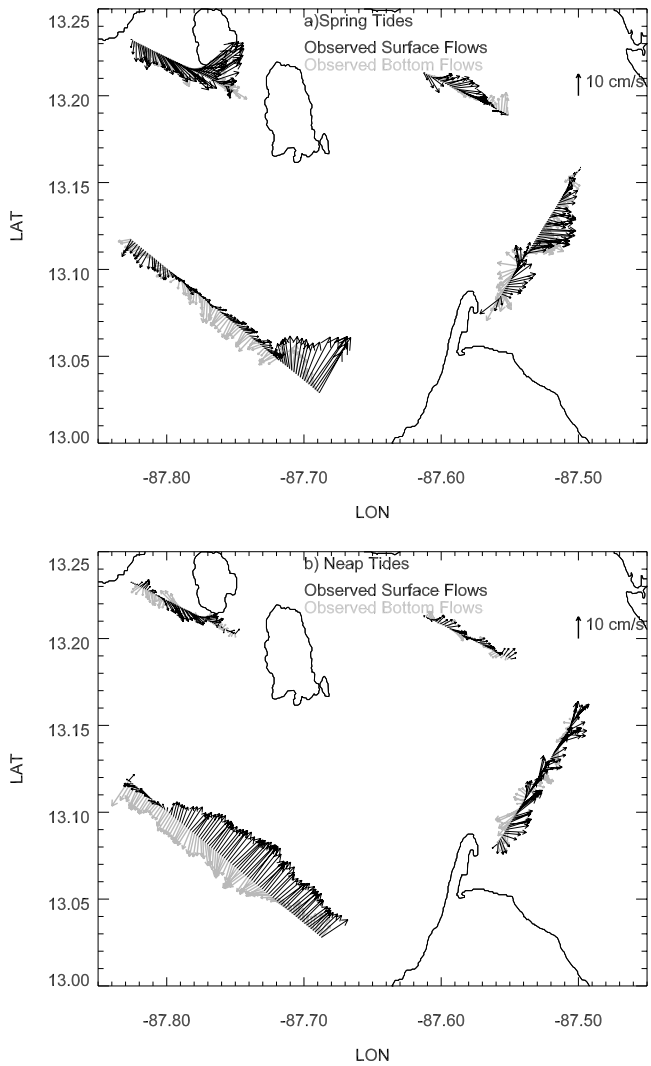

Figure 4. Mean surface and bottom flows obtained from a towed acoustic Doppler current profiler along four transects during one full tidal cycle: (a) spring tides and (b) neap tides.

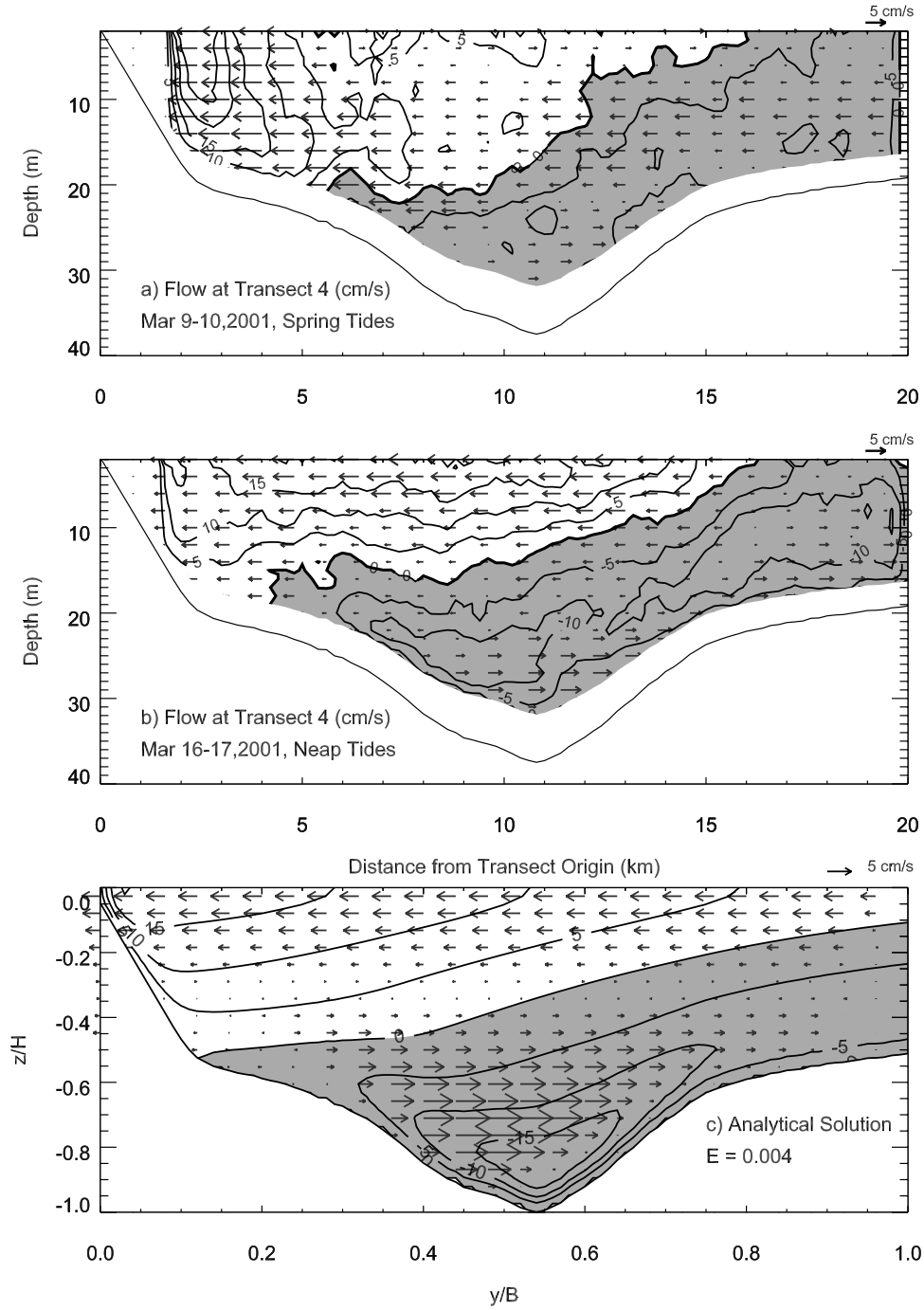

Figure 5. Cross section at the entrance to the gulf, looking seaward, showing the mean along-estuary and cross-estuary flow (cm s^{-1}) during the dry season at (a) spring tides, (b) neap tides, and (c) the analytical solution described in Appendix A. Shaded areas represent net outflows. Nicaragua is to the left.

tides. The analytical model results were obtained with prescribed surface slopes of 6×10^{-7} in both directions, which yielded dynamically consistent density gradients of 2.5×10^{-5} kg m^{-4}, similar to those observed. The resemblance between observed flow in neap tides and nearly geostrophic analytical results (low E) is remarkable. During spring tides the scaling of Table 2 should suggest additional influences from advective and frictional effects, but the use of the same along-estuary flow as representative for spring and neap tides (Figure 5, sectional mean outflow was not different between neap and spring tides) concealed those influences.

[20] The net volume inflow measured with the towed ADCP during spring tides was 1.4×10^4 m^3 s^{-1}, whereas the net volume outflow was 1.1×10^4 m^3 s^{-1}. In comparison, during neap tides the net volume inflow was 1.7×10^4 m^3 s^{-1} and the net volume outflow was 1.4×10^4 m^3 s^{-1}. The difference between volume inflow and volume outflow remained practically unchanged from spring to neap tides at 3000 m^3 s^{-1}. This volume surplus inside the gulf may be

Table 2. Scaling of the Main Forcing That Should Have Influenced the Net Flows at the Entrance to the Gulf of Fonseca (Transect 4) During Each Experiment[a]

	Dry Season		Wet Season	
Experiment	Spring Tides	Neap Tides	Spring Tides	Neap Tides
τ_x, Pa	0.008	0.007	0.04	0.04
τ_y, Pa	0.008	0.007	0.04	0.04
u, m s^{-1}	0.10	0.10	0.10	0.10
v, m s^{-1}	0.05	0.05	0.05	0.05
$\partial\rho/\partial x$, kg m^{-4}	2.0×10^{-5}	2.0×10^{-5}	1.5×10^{-5}	1.5×10^{-5}
$\partial\rho/\partial y$, kg m^{-4}	2.5×10^{-5}	2.5×10^{-5}	1.5×10^{-5}	1.5×10^{-5}
Along-estuary momentum ($\times 10^{-6}$ m s^{-2})				
fv	1.7	1.7	1.7	1.7
$gH/\rho\ \partial\rho/\partial x$	5.8	5.8	4.3	4.3
$\tau_x/\rho\ H$	0.3	0.2	1.3	1.3
$C_d u^2/H$	0.8	0.8	0.8	0.8
u^2/L	0.5	0.5	0.5	0.5
Across-estuary momentum ($\times 10^{-6}$ m s^{-2})				
fu	5.0	3.3	5.0	3.3
$gH/\rho\ \partial\rho/\partial y$	7.2	7.2	4.3	4.3
$\tau_y/\rho\ H$	0.3	0.2	1.3	1.3
$C_d v^2/H$	0.4	0.4	0.4	0.4
v^2/L	0.3	0.3	0.3	0.3

[a]The following values were used: $f = 3.3 \times 10^{-5}$ s^{-1}; $L = 20$ km; $C_d = 0.0025$; $g = 9.8$ m s^{-2}; $H = 30$ m; and $\rho = 1021$ kg m^{-3}.

canceled by (1) excess evaporation losses but is mostly accounted for by (2) the fact that a significant portion of the gulf entrance was not sampled. The mean flow distributions (Figures 5a and 5b) suggested that the unsampled portion of the entrance (~15 km) should have carried net outflows of ~0.02 m s^{-1} over a mean depth of 10 m, i.e., 3000 m^3 s^{-1}. Even though estimates of evaporation rates, on the basis of mass conservation, are within the error of our volume flow measurements, we may obtain an approximate estimate of the residence time by dividing the volume of the gulf (2.4×10^{10} m^3) by the volume inflow (1.4×10^4–1.7×10^4 m^3 s^{-1}), which was reasonably well represented in our measurements. This yielded an estimate of 16–20 days.

[21] The mean density and velocity profiles at the entrance of the gulf as well as the mean surface flow suggested an inverse estuarine circulation in the Gulf of Fonseca during the dry season. It is likely, however, that the system behaves as a salt plug estuary [e.g., *Wolanski*, 1986]. These types of estuaries feature a local salinity maximum within the embayment that may develop as evaporation rates compare to river discharge rates. River discharge was still present during our sampling period. Unfortunately, owing to the lack of a longitudinal section along the tributaries, we could not verify whether density increased from the mouth to the head up to a point where it decreased under the influence of freshwater discharge. At this time we can only hypothesize that we observed a salt plug estuary. During the dry season we had several types of evidence for near-surface flow into the Gulf of Fonseca. This near-surface inflow likely affected the water quality of the system and later reversed during the wet season.

4.2. Wet Season

[22] In the wet season the distribution of mean hydrographic variables was as expected from a regular estuary, where freshwater input exceeds freshwater losses. The distributions within each of the four transects showed density decreasing toward the north stations (Figures 6 and 7); that is, near-bottom density decreased from Nicaragua to El Salvador in transect 4 by 0.3 kg m^{-3} in 20 km. Transect to transect comparisons featured a decrease in mean salinity and density from transects 3–1 or from east to west in the lower gulf. The along-estuary density gradient was not resolved by our observations, but transect 3 reflected a northward decrease of salinity and density. There is some evidence that the horizontal density gradient reversed sign relative to the dry season and was expected to drive estuarine circulation.

[23] The mean flows measured with the towed ADCP showed surface outflows and bottom inflows (Figure 8). This is typical of gravitational circulation driven by the pressure gradient and balanced by Coriolis accelerations and friction. The observed exchange pattern was consistent from transect to transect, even though they were sampled sequentially and not simultaneously. Once again, the exchange patterns appeared more robust in neap tides than in spring tides. This was best illustrated in the outflows at transects 1 and 3 (Figure 8). Horizontal variability in the flow was observed during spring tides, most notably in transect 4; that is, net flows were more coherent throughout transect 4 in neap tides than in spring tides. In contrast, transects 1 and 3 featured similarly rich horizontal variability from neap to spring tides, which suggested that other forcing agents, in addition to the pressure gradient, tidal friction, and Coriolis accelerations, affected the net flow patterns. This is best illustrated by the sections at the entrance to the gulf.

[24] The cross sections of subtidal flows in transect 4, at the entrance to the gulf, illustrated surface outflow and bottom inflow (Figure 9). During spring tides the strongest outflow of the section appeared close to Nicaragua, on the opposite side where it would be expected from Coriolis's influences. The same situation of strongest outflow near Nicaragua was observed during neap tides. This distribution of net outflows may reflect the fact that the transect did not capture most of the outflow on the side of the gulf entrance next to El Salvador. In addition, the slope of the isotachs was of opposite sign to that expected from geostrophic dynamics. The sign of the isotachs slope may have been caused by increased frictional effects from wind forcing relative to the dry season. Wind speeds, measured onboard, oscillated between 3 and 5 m s^{-1} and peaked at 10 m s^{-1}, in a direction that tended to reinforce the gravitational circulation. The scaling of dynamic terms (Table 2) indicates that wind stresses were relevant in shaping the net exchange flows observed in both spring and neap tides of the wet season. In fact, it is possible that these net exchange flows reflected a pattern consisting of inflow in channel (upwind) and outflow over shoals (downwind), as obtained in the analytical results of *Csanady* [1973] and *Wong* [1994]. The possible outflow over the shoal off El Salvador was simply not sampled in the transect. Regardless of the transect coverage, the slope of the inflowing isotachs, the location of the core of maximum inflow, and the scaling of dynamic terms strongly suggested wind influences that should have increased frictional effects at the gulf entrance.

[25] Another interesting aspect of the net flow distributions at the entrance to the gulf during the wet season was

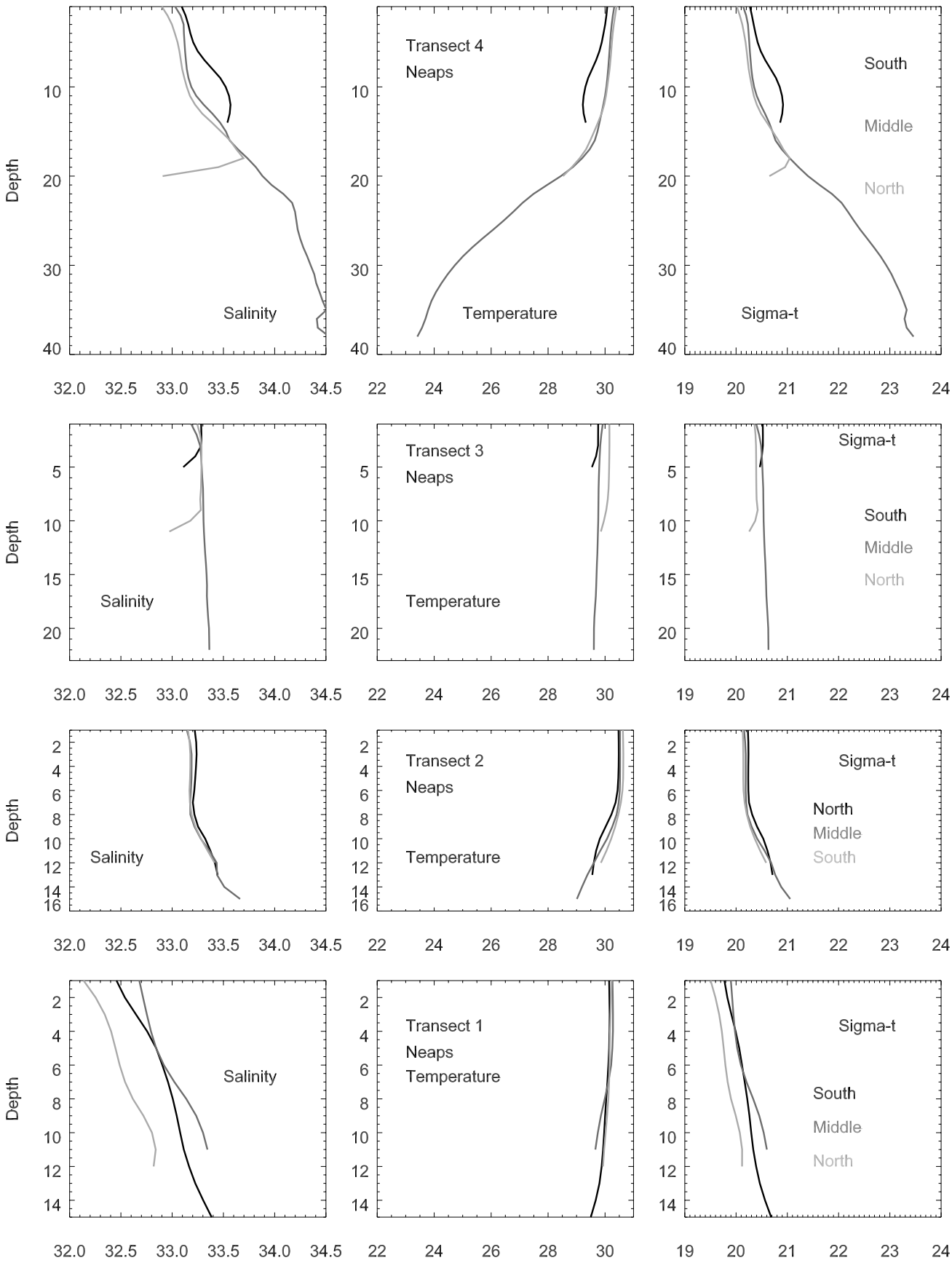

Figure 6. Same as Figure 2, but for the wet season neap tides.

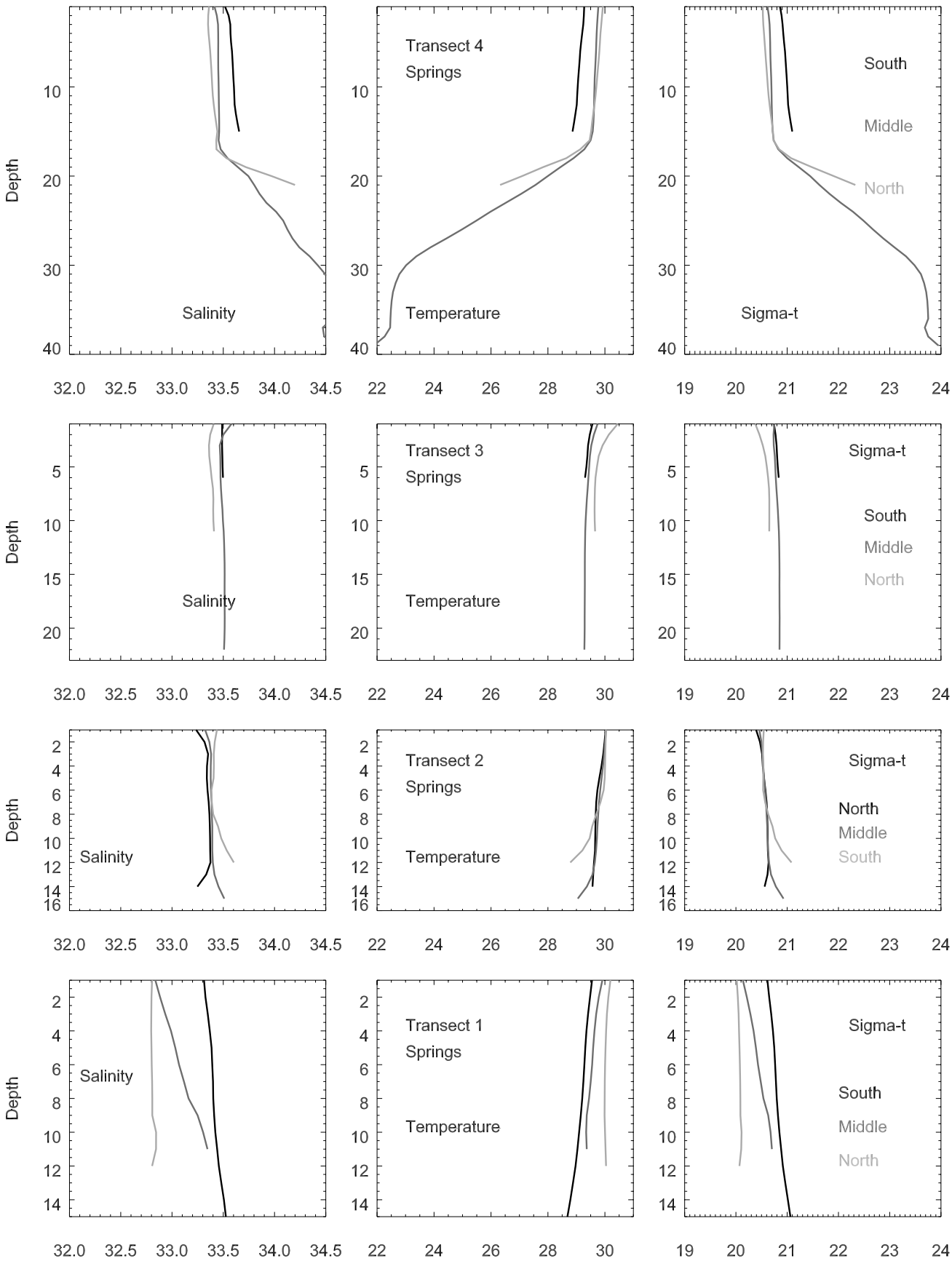

Figure 7. Same as Figure 6, but for spring tides.

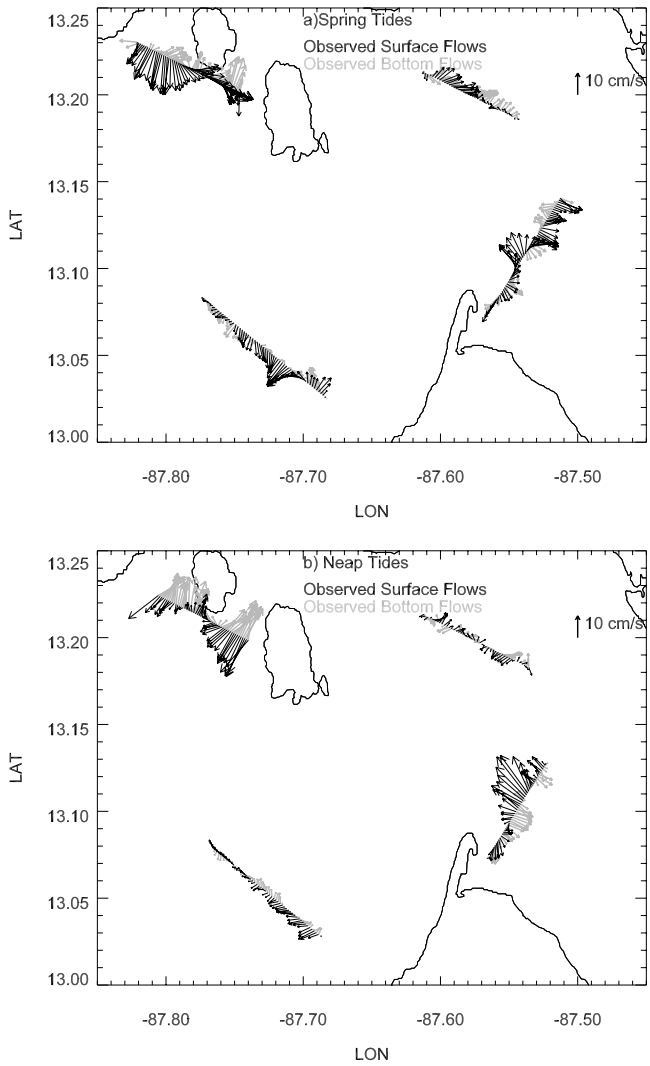

Figure 8. Same as Figure 4, but for the wet season.

that the area occupied by outflow was much smaller than that of inflow (Figure 9). Yet the opposite scenario was expected because of the surplus of water input to the system. In spring tides, volume outflow was 0.3×10^4 m^3 s^{-1} and volume inflow was 0.9×10^4 m^3 s^{-1}, whereas in neap tides volume outflow was 0.3×10^4 m^3 s^{-1} and volume inflow was 1.2×10^4 m^3 s^{-1}. These volume fluxes again indicated incomplete coverage of the outflow next to El Salvador and reflected increased volume exchange in neap tides relative to spring tides. Volume inflows were ~30% smaller than those measured in the dry season. This reduction in volume inflow to the gulf may have been related to the seaward barotropic pressure gradient associated with river input. The reduced volume inflows yielded residence times, following the procedure used for the dry season, of 23–31 days. Therefore it could be said that, in general, the residence time in the Gulf of Fonseca is between 2 weeks and 1 month.

5. Summary

[26] Observations obtained with a combination of sensors that had not been used in tropical estuaries, at least in the Americas, documented the seasonal reversal of circulation patterns in the Gulf of Fonseca, a tropical estuary of the Pacific coast of Central America. During the dry season the circulation at the entrance to the gulf resembled an inverse estuary, with near-surface waters entering the gulf and near-bottom waters leaving the gulf. This exchange pattern was modified by Coriolis accelerations. However, because of the persistent, yet weak, supply of fresh water to the gulf, it is likely that the gulf acts like a salt plug estuary during the dry season. The water exchange pattern was slightly modified from neap to spring tides as frictional effects increased and volume exchange decreased. In contrast, during the wet season the circulation at the gulf's entrance reflected typical estuarine conditions: outflow at surface and inflow at depth. During this period, wind forcing competed with Coriolis accelerations, as determined by the scaling of the terms and by the slope of the isotachs during both spring and neap tides. Once again, volume exchange increased from spring to neap tides as tidal friction decreased. On the basis of the volumes exchanged at the entrance to the gulf, we propose that its residence time is between 2 weeks and 1 month.

[27] The reversal of exchange patterns in an estuarine system has important implications for water quality. During the dry season, net surface inflows hold buoyant materials inside the system for longer periods than during the wet season. Also, during the dry season the ability of the system to flush is weaker than during the wet season because of volume losses related to evaporation. These issues remain to be explored with interdisciplinary studies in these types of systems.

Appendix A: Analytical Model

[28] The analytical model that generated the results of Figure 5c follows *Kasai et al.* [2000] and *Valle-Levinson et al.* [2003]. It solves for the nontidal or mean along-estuary u and transverse v flows produced by pressure gradients and modified by Coriolis and frictional influences. In a right-handed coordinate system (x, y, z), where x points seaward, y points across the estuary, and z points upward, the nontidal (or steady) momentum balance to be solved becomes a set of two differential equations:

$$-fv = -g\frac{\partial \eta}{\partial x} + \frac{g}{\rho_0}\frac{\partial \rho}{\partial x}z + A_z\frac{\partial^2 u}{\partial z^2},$$
$$fu = -g\frac{\partial \eta}{\partial y} + \frac{g}{\rho_0}\frac{\partial \rho}{\partial y}z + A_z\frac{\partial^2 v}{\partial z^2}, \quad \text{(A1)}$$

where f, g, ρ_0, ρ, η, and A_z are the Coriolis parameter, the gravity acceleration (9.8 m s^{-2}), the reference water density, the variable water density (kg m^{-3}), the surface elevation (m), and the vertical eddy viscosity homogeneous in z and y (m^2 s^{-1}), respectively. The set of equations (A1) may be represented in terms of a complex velocity $w = u + iv$, where $i^2 = -1$ is the imaginary number

$$gN - Dz = A_z\frac{\partial^2 w}{\partial z^2} - ifw. \quad \text{(A2)}$$

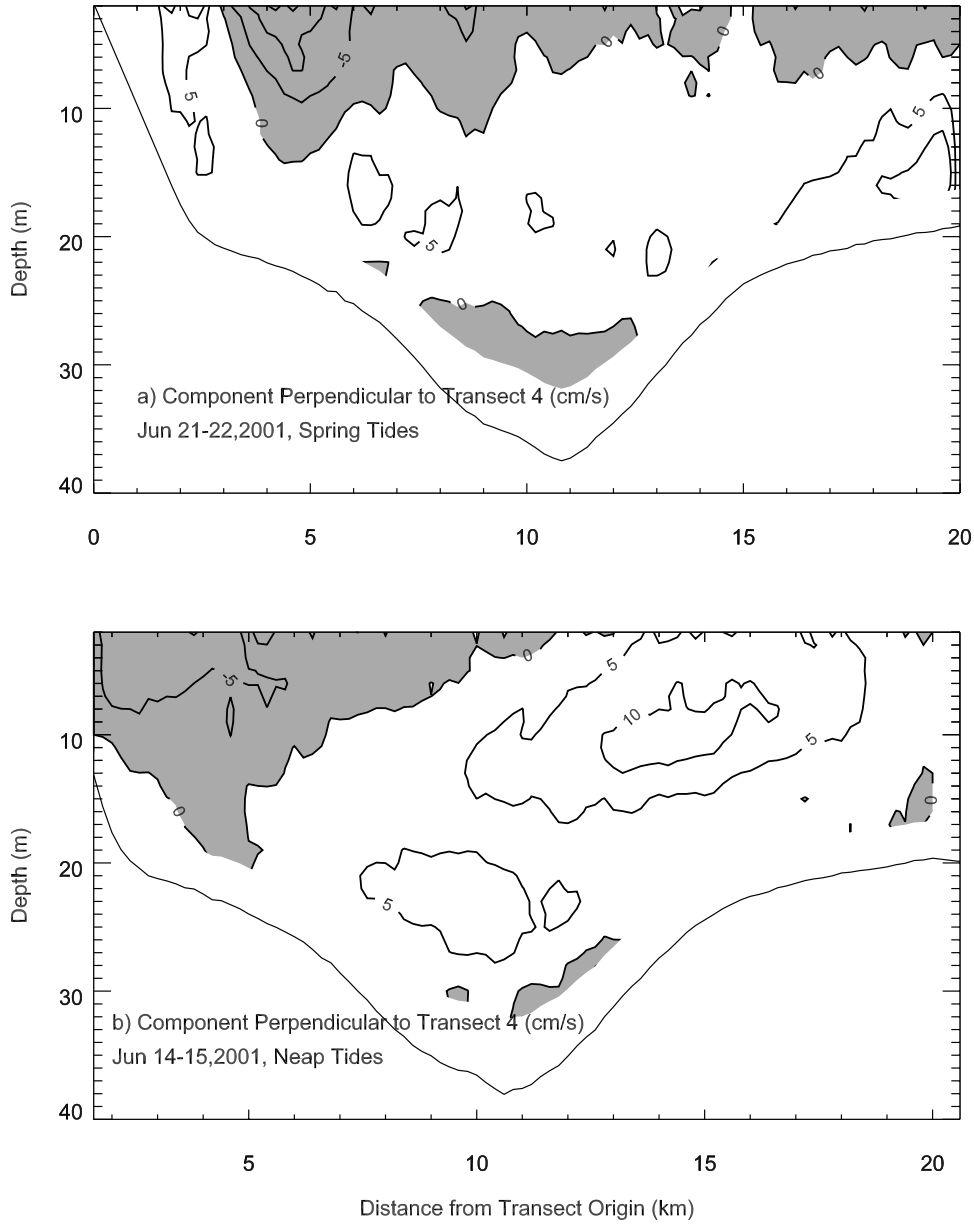

Figure 9. Cross section at the entrance to the gulf, looking seaward, showing the mean flow perpendicular to the sampling transect during the wet season at (a) spring tides and (b) neap tides. Shaded areas represent net outflows. Nicaragua is to the left.

In equation (A2), N and D represent the barotropic and baroclinic pressure gradients, respectively:

$$N = \frac{\partial \eta}{\partial x} + i\frac{\partial \eta}{\partial y};$$

$$D = \frac{g}{\rho_0}\left[\frac{\partial \rho}{\partial x} + i\frac{\partial \rho}{\partial y}\right];$$

and are assumed independent of depth. Then, the flow w has contributions from the sea level slope and from the horizontal density gradients, i.e.,

$$w(z) = gNF_1(z) + F_2(z), \tag{A3}$$

and F_1 and F_2 represent functions that depict the vertical structure of the barotropic (from sea level slope) and baroclinic (from density gradient) contributions to the flow. Using equation (A3), equation (A2) can then be rewritten as

$$\begin{aligned} \frac{\partial^2 F_1}{\partial z^2} - \frac{if}{A_z}F_1 &= \frac{1}{A_z}; \\ \frac{\partial^2 F_2}{\partial z^2} - \frac{if}{A_z}F_2 &= -\frac{Dz}{A_z}. \end{aligned} \tag{A4}$$

Assuming, as boundary conditions, no stress at the surface ($\partial F_1/\partial z = \partial F_2/\partial z = 0$ at $z = 0$) and no slip at the bottom (F_1 and $F_2 = 0$ at $z = -H$) and that the horizontal density

gradient is independent of depth, the solution of equation (A4) is

$$F_1 = \frac{i}{f}\left[1 - \frac{\cosh(\alpha z)}{\cosh(\alpha H)}\right];$$
$$F_2 = \frac{iD}{f\alpha}\left[(e^{\alpha z} - \alpha z) - \left(e^{-\alpha H} + \alpha H\right)\frac{\cosh(\alpha z)}{\cosh(\alpha H)}\right]. \quad \text{(A5)}$$

In this solution the parameter α equals $(1 + i)/D_E$, where D_E is the Ekman layer depth $[2A_x/f]^{1/2}$. Equations (A5) and (A3) require prescription of the sea level slope N and the eddy viscosity A_z and a density gradient D that is dynamically consistent with N. In order to derive the value of D, we use a boundary condition that assumes no net volume flux along or across the channel [*Kasai et al.*, 2000], i.e.,

$$\int_0^B \int_{-H}^0 w\, dz\, dy = 0, \quad \text{(A6)}$$

where B is the estuary's width. The value of D that satisfies a prescribed N is

$$D = -\frac{\alpha g I_1 \int_0^B N(y)dy}{I_2}$$
$$= \frac{\alpha g \int_0^B N(y)\left[\left(e^{-\alpha H} + \alpha H\right)\tanh(\alpha H) - \left(1 - e^{-\alpha H} + \alpha^2 H^2/2\right)\right]dy}{\int_0^B [\tanh(\alpha H) - \alpha H]dy}. \quad \text{(A7)}$$

Prescribing N $(= 6 \times 10^{-7}\{1 + i \exp[-(y/B - 1)^2]\})$ and A_z $(= 2 \times 10^{-4}\ \mathrm{m^2\ s^{-1}})$, and with H as any function of y, the solution to equation (A3) is obtained with equations (A5) and (A7) and is portrayed in Figure 5c, for which D is $2.5 \times 10^{-7}(1 + i)$. The solutions may be cast in terms of the vertical Ekman number $E = A_z/(fH^2_{\max})$, where $H_{\max}$ is the maximum depth.

[29] **Acknowledgments.** This study was funded by the U.S. National Oceanic and Atmospheric Administration's (NOAA) National Ocean Service (NOS) as part of the restoration efforts of the U.S. Department of Commerce to the countries impacted by Hurricane Mitch in 1998. Funding from U.S. NSF Project 9983685 to AVL is gratefully acknowledged. A large number of people made this study possible. The coordination of C. Oberbeck in El Salvador, M. Drazba in Nicaragua, and especially M. M. Alonzo in Honduras at the USAID offices was pivotal for the permits and logistics among the three countries that share the gulf. The captain, O. Cepeda, and crew, F. Cifuentes and R. Dennison, of the *Nolan Ponce* did an outstanding job under the very demanding sampling schedule. Thanks to C. E. Whitaker of Empresa Portuaria of Nicaragua for providing the vessel. The assistance of M. M. Alonzo, A. Medina, E. Muñoz, and E. Mejía in facilitating transportation and coordination within Honduras is greatly appreciated. The data collection would not have been possible without the expertise and participation of C. Reyes, R. Sanay, H. Sepulveda, J. L. Blanco, D. Salas, H. C. Kim, D. Dwyer, E. Demir, and R. Taylor; their help is greatly appreciated. For radar data collection we are also very thankful to C. Kazan, and for data processing and distribution we are thankful to C. Whelan and L. Pedersen from CODAR. The comments of J. Toole and two anonymous reviewers are greatly appreciated.

References

Csanady, G. T., Wind-induced barotropic motions in long lakes, *J. Phys. Oceanogr.*, *3*, 429–438, 1973.

Fang, T., and L. Piegl, Algorithm for Delaunay triangulation and convex hull computation using a sparse matrix, *Comput. Aided Design*, *24*, 425–436, 1992.

Fang, T., and L. Piegl, Delaunay triangulation using a uniform grid, *IEEE Comput. Graphics Appl.*, *13*, 36–47, 1993.

Geyer, W. R., and G. A. Cannon, Sill processes related to deep water renewal in a fjord, *J. Geophys. Res.*, *87*, 7985–7996, 1982.

Geyer, W. R., and R. Signell, Measurements of tidal flow around a headland with a shipboard acoustic Doppler current profiler, *J. Geophys. Res.*, *95*, 3189–3197, 1990.

Gill, A. E., *Atmosphere-Ocean Dynamics*, 661 pp., Academic, San Diego, Calif., 1982.

Griffin, D. A., and P. H. LeBlond, Estuary/ocean exchange controlled by spring-neap tidal mixing, *Estuarine Coastal Shelf Sci.*, *30*, 275–305, 1990.

Haas, L. W., The effect of the spring-neap tidal cycle on the vertical salinity structure of the James, York and Rappahanock Rivers, Virginia, USA, *Estuarine Coastal Shelf Sci.*, *5*, 485–496, 1977.

Joyce, T. M., On in situ "calibration" of shipboard ADCPs, *J. Atmos. Oceanic Technol.*, *6*, 169–172, 1989.

Kasai, A., A. E. Hill, T. Fujiwara, and J. H. Simpson, Effect of the Earth's rotation on the circulation in regions of freshwater influence, *J. Geophys. Res.*, *105*, 16,961–16,969, 2000.

Nunes, R. A., and G. W. Lennon, Episodic stratification and gravity currents in a marine environment of modulated turbulence, *J. Geophys. Res.*, *92*, 5465–5480, 1987.

Nunes Vaz, R. A., G. W. Lennon, and J. R. de Silva Samarasinghe, The negative role of turbulence in estuarine mass transport, *Estuarine Coastal Shelf Sci.*, *28*, 361–377, 1989.

Nunes Vaz, R. A., G. W. Lennon, and D. G. Bowers, Physical behaviour of a large, negative or inverse estuary, *Cont. Shelf Res.*, *10*(3), 277–304, 1990.

Salas-Monreal, D., Sea level slopes and volume fluxes produced by atmospheric forcing in Chesapeake Bay, M.S. thesis, 95 pp., Old Dominion Univ., Norfolk, Va., 2002.

Signell, R. P., and C. K. Harris, Modeling sandbank formation around tidal headlands, in *Estuarine and Coastal Modeling: Proceedings of the 6th International Conference*, edited by M. Spaulding and H. L. Butler, pp. 209–222, ASCE Press, Reston, Va., 2000.

Valle-Levinson, A., and L. P. Atkinson, Spatial gradients in the flow over an estuarine channel, *Estuaries*, *22*(2A), 179–193, 1999.

Valle-Levinson, A., J. A. Delgado, and L. P. Atkinson, Reversing water exchange patterns at the entrance to a semiarid coastal lagoon, *Estuarine Coastal Shelf Sci.*, *53*, 825–838, 2001.

Valle-Levinson, A., C. Reyes, and R. Sanay, On the effects of bathymetry, friction and rotation on estuary/ocean exchange, *J. Phys. Oceanogr.*, *33*, 2375–2393, 2003.

Wolanski, E., An evaporation-driven salinity maximum zone in Australian tropical estuaries, *Estuarine Coastal Shelf Sci.*, *22*, 415–424, 1986.

Wong, K.-C., On the nature of transverse variability in a coastal plain estuary, *J. Geophys. Res.*, *99*, 14,209–14,222, 1994.

K. T. Bosley, National Ocean Service, National Oceanographic and Atmospheric Administration, 808 Principal Court, Chesapeake, VA 23320, USA. (kate.bosley@noaa.gov)

A. Valle-Levinson, Center for Coastal Physical Oceanography, Department of Ocean, Earth and Atmospheric Sciences, Old Dominion University, Norfolk, VA 23529, USA. (arnoldo@ccpo.odu.edu)